Solubility–spinnability map and model for the preparation of fibres of polyethylene (terephthalate) using gyration and pressure

Suntharavathanan Mahalingam [a],*, Bahijja Tolulope Raimi-Abraham [b], Duncan Q.M. Craig [b], Mohan Edirisinghe [a]
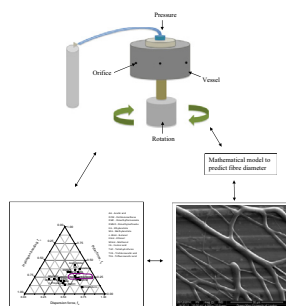
[a] *Department of Mechanical Engineering, University College London, Torrington Place, London WC1E 7JE, UK*
[b] *University College London School of Pharmacy, 29-39 Brunswick Square, London WC1N 1AX, UK*

HIGHLIGHTS

- Gyration under pressure was used to spin PET nanofibres.
- Teas graph was mapped to identify the solubility–spinnability region.
- Scaling law was found for relationship between polymer concentration and viscosity.
- Structural evolution in PET nanofibres is explained.
- Mathematical model has been developed to predict fibre diameter.

GRAPHICAL ABSTRACT

ABSTRACT

The selection of a solvent or a solvent system is a fundamental and a crucial step in spinning fibres using a selected process. Solvent selection determines the critical minimum polymer concentration and the critical minimum chain entanglement which allows the spinning of nanofibres rather than other hybrid morphologies such as beaded structures. Pressurised gyration, which simultaneously combines the use of gas pressure and rotation, is used as the processing and forming route for spinning fibres in this work. This study investigates 23 different solvents and solvent systems spread on a wide area of a Teas graph and able to dissolve the functional polymer polyethylene (terephthalate) (PET) and spin products by the application of pressurised gyration. The results are mapped on a Teas graph to identify the solubility–spinnability region. Based on this solubility–spinnability region, various solvents and binary solvent systems that allow the making of PET fibres are suggested. Scaling laws for the relationship between polymer concentration and specific viscosity are identified. The structural evolution in the fibres prepared is elucidated. For the first time, a mathematical model to scale fibre diameter with respect to flow properties and processing parameters encountered in pressurised gyration has been successfully developed.

© 2015 The Authors. Published by Elsevier B.V. This is an open access article under the CC BY license (http://creativecommons.org/licenses/by/4.0/).

1. Introduction

The rise in demand for nanofibrous structures across a wide range of industries demands innovative manufacturing methods with mass production capabilities. It is this issue that has proved to be a major barrier to translational development; scale up using the currently available production techniques is extremely challenging. The current state-of-the-art technologies, (e.g. electrospinning, blowing and centrifugal spinning) cannot produce nanofibrous structures consistently, reliably, robustly and cost effectively [1]. All three methods have striking limitations.

Solution electrospinning can generate uniform nanofibres of tailored morphologies and functionalities from a diverse range of materials, but suffers from low productivity. If melt (rather than solution) electrospinning is used, fibres generated are largely limited to the submicrometre diameter range. Centrifugal spinning methods produce uniaxially aligned 3D nanofibrous bundles from solutions in a cylindrical spinneret using centrifugal force; these suffer from complexity in the spinneret design which affects productivity and thus are not economical. Even nozzleless centrifugal spinning such as Forcespinning™ has yet to make a significant impact. Melt or solution blowing relies on mechanical drawing to extrude fibres using a high velocity air stream, it benefits from high productivity, but can only generate uniform fibres in the micrometre scale and fails to consistently produce nanofibres. The above scenarios demand new advances in nanofibre and nanofibrous structure manufacturing processes. Novel manufacturing routes should have capabilities to process multi-functional nanofibres and nanofibrous structures that can safely, consistently and cost-effectively be up-scaled, and this is offered by pressurised gyration, which has been recently used to generate nanofibres from different polymers [1–5].

Pressurised gyration relies on application of centrifugal force and dynamic fluid flow in a sealed cylindrical vessel containing polymer solution to jet out fibres. In a typical pressurised gyration process, the surface tension force of the polymer solution is overcome by the centrifugal force and dynamic fluid flow to form the instability at the liquid–air interface. Subsequently the solvent evaporates in the fibre jets travelling between the vessel and the collector and solidifies to form nanofibres. The resultant fibre size, fibre size distribution and morphology depend on rotating speed of the vessel, working pressure and polymer solution concentration [1,2,4]. The optimisation of these parameters is significant in order to obtain continuous nanofibres with well defined morphology and properties. The majority of studies therefore have focused on optimisation of these parameters regardless of the solution properties. The selection of the solvent or mixed solvents to dissolve the polymer is one of main factors which can influence the solution properties and spinnability of nanofibres in pressurised gyration.

Polymer–solvent interaction determines the polymer solution properties and is significantly affected by solubility afforded by the solvent [6]. A higher solubility forms strong polymer–solvent interactions where polymer chains swell and expand to maximise intermolecular interactions. Poor solubility favours polymer–polymer interactions where polymer chains contract and stay closer to each other [6]. Solubility is also affected by temperature and the chemical composition of the polymer and the solvent [6]. Manipulation of the solvent solubility influences the polymer chain conformation, viscoelasticity, critical minimum concentration, fibre size, crystallinity, tensile strength, aspect ratio and morphology of polymeric fibres [7–10]. Thus, the selection of solvent and solvent system for a particular polymer plays a pivotal role in determining the above properties and is fundamental to the success of pressurised gyration to form nanofibres.

Solubility parameters are used to identify a suitable solvent and/or solvent system for a particular polymer to spin nanofibres. These solubility parameters are useful in predicting the solubility of polymer in various solvents, thus they are crucial for designing formable formulations. Among the large variety of solubility parameters, the ternary solubility diagram, generally referred to as Teas graph has attracted much interest in the literature for its usefulness in selecting solvents for making polymer solutions [11–13]. It has a distinct advantage compared other solubility parameters such as classical solubility parameters (Hildebrand solubility parameter) and Hansen three component solubility parameters. In classical solubility parameters only the London dispersion forces are taken into consideration [14,15]. However, the solvents

have a permanent dipole, thus it is essential to consider dipole force in addition to dispersion force in the polymer–solvent interaction. In addition, hydrogen bonding plays a significant role in polymer solubility [16]. The fractional cohesion parameters f_d, f_h, and f_p where d, h and p represents dispersion force, hydrogen bonding and polar force, respectively, are mathematically derived from Hansen solubility parameters δ_d, δ_h and δ_p, respectively and presented on a 2D graph, allowing more straightforward analysis of the solubility behaviour of the polymer of interest. Previous studies have indicated that a Teas graph shows a reasonable degree of accuracy and practicality for providing insights on the solubility of many polymers [11–13].

Polyethylene (terephthalate) (PET) is a class of synthetic polyesters widely used in automotive and functional applications because of its excellent thermal and mechanical properties. These properties of PET also make it a potential candidate in applications such as filtration, membranes and protective clothing [17–19]. PET fibres have been used in tissue engineering scaffolds and as drug delivery vehicles [20]. PET is synthesised from terephthalic acid (HOOC–C_6H_4–COOH) and ethylene glycol (HO–C_2H_4–OH) and has a semi-crystalline structure composed of crystalline and amorphous regions [21]. Much research has been done to form PET fibres through solvent and solvent-less routes, such as melt spinning, for a broad range of applications [22–24]. However, the solubility–spinnability map has not been developed for this important polyester which has extensive applications in many areas. This study investigates the solubility–spinnability of PET subjected to pressurised gyration in various solvent systems. In this work, a wide variety of solvents and solvent systems with diverse solubility parameters have been used to map the solubility–spinnability of PET. In addition, critical minimum concentration needed to form fibres in the good solvents has been determined. The selection of solvents and the spinnability of PET are correlated with the critical minimum entanglement concentration and the morphology of the products in pressurised gyration. The structural evolution in the fibres prepared is explained. A mathematical model has been developed based on rotational and blowing frames to scale the fibre diameter with flow properties and forming parameters. The predicted fibre diameter is compared with experimentally observed values.

2. Materials and methods

2.1. Materials

PET (M = 100,000 g/mol) was obtained from Sigma Aldrich (Poole, UK) and used in this investigation.

Acetic acid (AA), dichloromethane (DCM), dimethylformamide (DMF), dimethylsulfoxide (DMSO), ethylacetate (EA), methylacetate (MA), butanol (n-BtOH), ethanol (EtOH), methanol (MtOH), formic acid (FA), tetrahydrofuran (THF), glycerol, n-propanol, chloroform, acetonitrile, acetone, trichloroacidic trichloro acetic acid (TCA) and trifluoro acetic acid (TFA) were obtained from Sigma Aldrich (Poole, UK). All reagents were analytical grade and were used as received.

2.2. Mapping the solubility region of PET on the Teas graph

Solubility of a selection of 20 diversely positioned solvents on the Teas graph was tested with various concentrations of PET (5, 10, 15, 20 and 25 wt%) at atmospheric pressure and ambient conditions (temperature ~20 °C and relative humidity ~40%). Fractional cohesion parameters based on Barton was used to identify the solvent positions on Teas graph [25]. The degree of swelling or dissolution was visually assessed after stirring for 10 min,

30 min and 24 h, respectively. Solubility observed was categorised and recorded as insoluble, partial and high, based on the time taken for PET to dissolve in a solvent to form a homogenous solution. The solubility map of PET was identified by drawing a contour around the solubility test results of the selected solvents on the Teas graph.

2.3. Selection and testing of binary solvent systems

The proportions of the solvents mixed were determined geometrically based on the Teas graph using a method similar to the lever rule as illustrated by Burke and Jensen [26]. In the map it has been done by a line which joins the positions of the two selected solvents (e.g. A and B) on the Teas graph. If this line crosses the solubility region of the polymer, a point in this line (P) that can be tested is identified. The proportions of each solvent component in the system is calculated by volume fraction of solvent A = the length BP/length AB and volume fraction of B = length AP/length AB. The solubility results of mixed solvents using this method were compared with predictions drawn from the Teas graph.

2.4. Pressurised gyration

The experimental set up operating at ambient temperature used in this study is shown in Fig. 1. It consists of a rotary aluminium cylindrical vessel (~60 mm in diameter and ~35 mm in height) containing 20 orifices on its face. The size of one orifice is 0.5 mm. The vessel and orifice dimensions (including the number of orifices) can be varied to suite. One end of the vessel is connected to a motor which can generate speeds up to 36,000 rpm via a rotary joint. The other end is connected to a gas stream (e.g. N_2), the pressure of which can be varied up to 3×10^5 Pa. The high speed of the rotating vessel forms a polymer solution jet. This jet subsequently stretches into fibres through an orifice. This stretching can be enhanced by blowing of gas into the vessel. The formed polymer solution jet evaporates the solvent to generate the fibres. To facilitate the collection of polymeric fibres there is a stationary collector made of aluminium foil placed around the spinning vessel.

2.5. Characterisation

Zero-shear and solvents viscosities were measured using a Brookfield viscometer. Viscosity data were collected at the ambient temperature (~20 °C).

The morphology of fibres formed was studied by optical microscopy (Nikon Eclipse ME600) and scanning electron microscopy (SEM, Hitachi S-3400n), the latter at an accelerating voltage of
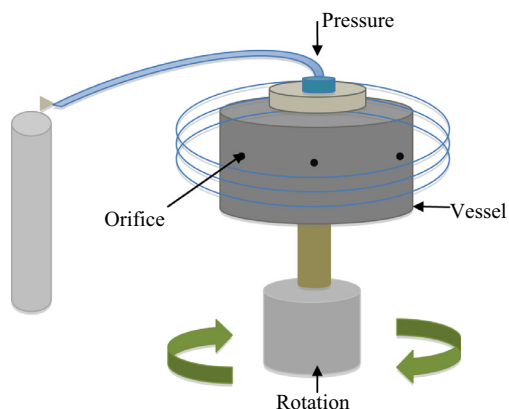

Fig. 1. Schematic diagram illustrating the experimental set-up used for pressurised gyration.

5 kV. The samples were coated with gold using a sputtering machine (Edwards Sputter S1 50B) for 150 s to minimize minimise charging effects prior to imaging. Statistical analysis on average fibre diameter and diameter distribution of nanofibres was obtained from SEM images. The fibre diameter was calculated using high magnification images with IMAGE J software using ~100 measurements which were made at different locations of the coated samples to calculate the average fibre diameter. The results were combined with the solubility map on the Teas graph to produce a spinnability–solubility map for PET.

Microstructural developments in the PET nanofibres during stepwise annealing was monitored with a differential scanning calorimeter (DSC). Thermograms were obtained using a DSC (PerkinElmer) under nitrogen atmosphere at a scanning rate of 10 °C/min. Thermogravimetric analysis (TGA) on the nanofibres was conducted using a PerkinElmer thermogravimetric analyser.

X-ray diffraction patterns of as prepared nanofibres and annealed nanofibres (up to 200 °C) were obtained with a RigaKu D/Max-BR diffractometer operating at 40 kV and 30 mA, over the 2θ range 5–60° with Cu K_α radiation.

3. Results and discussion

3.1. Solubility and the spinnability of PET using pressurised gyration

The development of a suitable solvent and solvent system for a particular polymer that could be processed using pressurised gyration to form nanofibres is crucial step in this process. Previous research on pressurised gyration was not primarily concerned with this step. In those experiments polymers were prepared in solvents that would jet out nanofibres, avoiding polymer bead formation. It is also noteworthy that no clear standard has been established for judging whether a solvent of high solubility for a polymer will produce a good solution for pressurised gyration.

Considering these facts, in this work we explored the solvent solubility and suitability to spin nanofibres from a polymer solution subjected to pressurised gyration. If the polymer solution in pressurised gyration generates continuous nanofibres with uniform morphology that is considered to be good spinnability. In addition, minimal bead-on-string fibre morphology was observed in the products. Table 1 illustrates the solubility of PET in various solvents and its spinnability in the pressurised gyration process based on Barton solubility parameters. By combining the solubility and spinnability, a solvent with high solubility for PET produced nanofibres whereas a solvent with partial solubility formed only polymer beads or droplets from 20 wt% PET polymer solutions. This differs with results obtained by Luo et al. [11] who obtained beads and droplets for the solvent with high solubility for 60 wt% PMSQ polymer in a spinning process. On the other hand, they reported that polymer with partial solubility in solvents produced more uniform fibres and showed that to spin nanofibres using PMSQ the polymer concentration needed to be greater than 60 wt% for solvents with high solubility. Another report by Shenoy et al. [27] indicated that for polyvinyllidene fluoride solutions in acetone, a poor solvent, can form fibres with a concentrations as low as 7.5 wt%; whereas a concentration of 30 wt% was needed in a good solvent, DMF, to form fibres. These contradictions, may be caused by the fact on each occasion a different polymer was studied and their viscosity-solution concentration profiles may generate different products depending on the process used. Thus, for a given process, the development of a suitable protocol (such as Teas graph) for a polymer to successfully generate fibres is a logical step forward.

The data given in Table 1 have been mapped as a Teas graph and the spinnability region is marked as a contour as shown in Fig. 2.

Table 1
PET solubility, fibre formability by pressurised gyration and solubility parameters of solvents used in this work. Fractional solubility parameters are based on Barton [25].

Solvent	PET solubility	Formability in pressurised gyration	$100f_d$	$100f_p$	$100f_h$
Acetic acid	Insoluble	–	40	19	41
Acetone	Insoluble	–	50	37	13
Chloroform	Insoluble	–	67	10	23
Dichloromethane	Partial	Beads	59	21	20
Dimethylformamide	Insoluble	–	41	32	27
Dimethylsulfoxide	Insoluble	–	37	33	30
Ethanol	Insoluble	–	36	19	45
Ethyl acetate	Insoluble	–	51	32	17
Formic acid	Partial	Beads	33	20	47
Methanol	Insoluble	–	31	23	46
Methyl acetate	Insoluble	–	45	36	19
Tetrahydrofuran	Partial	–	55	22	23
Water	Insoluble	–	19	22	58
n-Butanol	Insoluble	–	43	14	43
Acetonitrile	Insoluble	–	41	43	16
Glycerol	Insoluble	–	26	22	52
n-Propanol	Insoluble	–	40	16	44
Trifluoro acetic acid	Highly soluble	Nanofibres	50	26	24
Trichloro acetic acid	Highly soluble	Nanofibres	52	24	24

The solvents within this region can dissolve the PET polymer used in this work and have the ability to form nanofibres. Out of the 23 solvents tested, those in the bottom left to contoured region have strong hydrogen bonding, moderate to high dispersion force and low polar force. These solvents were unable to dissolve the PET pellets. The contour region has strong hydrogen bonding, strong dispersion force and high polar force. The dissolution of highly polar polymers in highly polar solvents involves two main processes. Initially, the breaking up of polar–polar bonds happen followed by the formation of new polar–polymer bonds. Moreover, solvent molecules first penetrate into polymer chains under the dominant influence of the entropic effect and break up the physical bonds between the polymer molecules, then the physical bonds between the solvent molecule and the polymer is newly formed in which the enthalpic effect is dominant [28]. However, it is interesting to note that solvents with a strong polar force other than those in the contour region were unable to fully dissolve the PET pellets. This indicates that not only the polar term governs the dissolution

process of PET polymer but also the dispersion forces and hydrogen bonding determine its solubility. These observations are different to those of Eom and Kim [28] and Liu et al. [29] where they showed that the polar term governs the individual solubility of the poly-acrylonitrile polymer [28] and the polar component was most important in solubility of polymethylmethacrylate [29]. However, other reports have showed that each force that forms a Teas graph is essential in determining the solvent–polymer interaction and the solubility of a polymer [11–13].

3.2. Binary solvent selection for spinning PET nanofibres

In addition to selecting a suitable single solvent for dissolving and spinning PET nanofibres by pressurised gyration, the Teas graph has been used for choosing a binary solvent system. For this purpose, a solvent with a high solubility for PET (i.e. TFA) and a non-solvent for PET were selected and a line is constructed to connect the positions of these solvents in the Teas graph (Fig. 3). It is
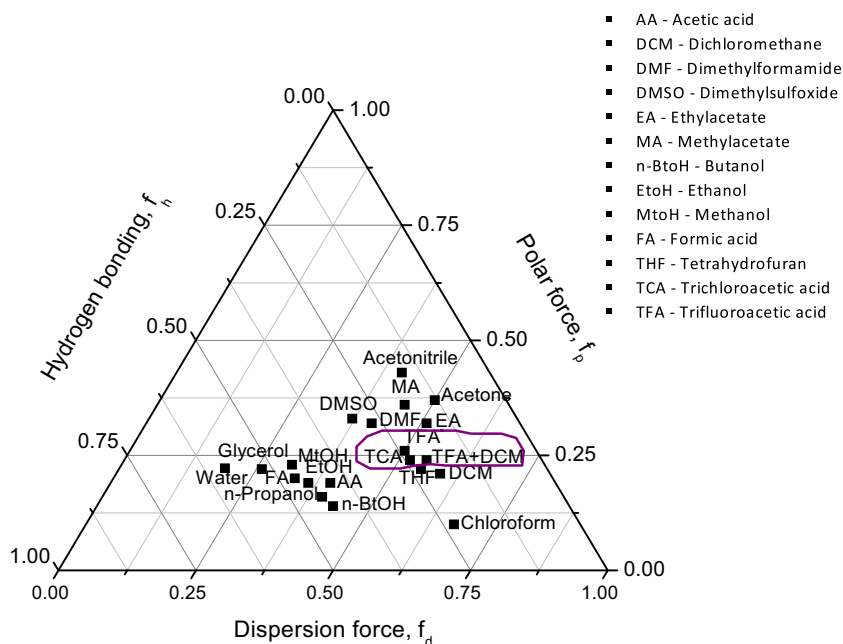

■ AA - Acetic acid
■ DCM - Dichloromethane
■ DMF - Dimethylformamide
■ DMSO - Dimethylsulfoxide
■ EA - Ethylacetate
■ MA - Methylacetate
■ n-BtoH - Butanol
■ EtoH - Ethanol
■ MtoH - Methanol
■ FA - Formic acid
■ THF - Tetrahydrofuran
■ TCA - Trichloroacetic acid
■ TFA - Trifluoroacetic acid

Fig. 2. Solubility–spinnability map of PET based on the ternary fractional parameter solubility diagram. A 20 wt% PET concentration was used. Conditions were atmospheric pressure, ~20 °C and relative humidity ~40%. It also indicates how the binary solvent systems were selected for spinning nanofibres by pressurised gyration.
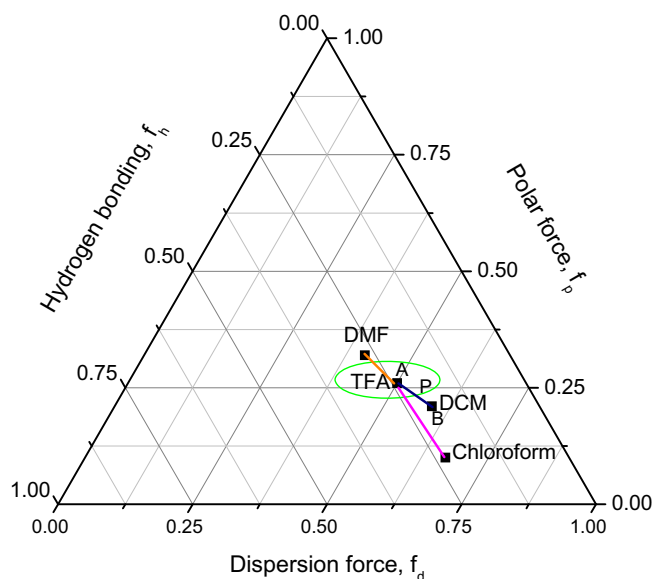
Fig. 3. Determination of binary solvent systems based on solubility–spinnability map of PET constructed using the ternary fractional parameter solubility diagram. A 20 wt% PET concentration was used. Conditions were atmospheric pressure, ∼20 °C and relative humidity ∼40%. As an example the binary solvent system TFA–DCM is considered.

also based on the theory that the selected binary solvent system should dissolve the PET and the solubility parameter of the combined solvent should be closer to the solvent that dissolves the PET to allow the formation of the nanofibres. Thus, the new Teas graph has important practicality in solvent selection for formation of nanofibres by pressurised gyration. The volume of solvents for the formation was calculated using the method described in Section 2.3. This empirical method to determine the solubility and selection of solvents for a particular polymer is invaluable as even a non-solvent for PET could be used to form nanofibres with the binary solvent system. Based on this protocol the solvent ratios for the binary solvent systems were determined. For TFA + DCM the ratio was 1:1, for TFA + CHCl₃ and TFA + DMF the ratio was 4:1. The binary solvent system consisting of TFA and DCM (1:1) has f_d, f_p, and f_h values of 54.5, 23.5 and 22, respectively (Table 2). On the Teas graph this is very close to the location of TFA which dissolves the PET and hence the binary solvent system is also expected to dissolve the PET.

3.3. Critical PET concentration

The plots of specific viscosity (η_{sp}) given by $\eta_o/\eta_s - 1$, where η_o and η_s are zero shear viscosity and solvent viscosity, respectively, versus the weight percentage of PET in the solutions investigated are shown in Fig. 4. Increase of the weight percentage of PET in TFA, TCA, TFA + DCM, TFA + DMF and TFA + CHCl₃ increased the specific viscosities of polymer solutions. There are two slopes observed for each plot representing the semi-dilute unentangled

Table 2
An illustration showing how fractional parameters of a solvent mixture can be calculated using fractional parameters of the solvent components.

Solvent	$100f_d$	$100f_p$	$100f_h$
TFA	50	26	24
DCM	59	21	21
TFA:DCM	$f_d = 1/$	$f_p = 1/$	$f_h = 1/$
(1:1)	2(50 + 59) = 54.5	2(26 + 21) = 23.5	2(24 + 21) = 22.5

for low concentrations and semi-dilute entangled for higher concentrations. At low concentrations the slope is 2.3, 2.3 and 2.1, 1.9, 1.7 for TFA, TCA, TFA + DCM, TFA + CHCl₃ and TFA + DMF solvents, respectively (Table 3). Higher concentrations give slope values of 3.9, 3.7, 3.5, 3.7 and 3.7 for TFA, TCA, TFA + DCM, TFA + CHCl₃ and TFA + DMF solvents, respectively (Table 3). For a linear polymer in a good solvent, the specific viscosity η_{sp} is proportional to $C^{1.25}$ in the semi-dilute unentangled regime and η_{sp} is proportional to $C^{4.25–4.50}$ in the semi-dilute entangled regime [30]. In polyimide solutions, the specific viscosity dependence on concentration changed from $C^{1.11}$ to $C^{4.42}$ at a concentration, C_e, of 18.3 wt% and this is the critical chain entanglement concentration [31]. Linear and the branched polyesters with different molecular weight showed that in the unentanglement regime η_{sp} is proportional to $C^{1.39}$ and in the entanglement regime, η_{sp} is proportional to $C^{2.7}$ [32]. Thus, the derived scaling values for PET in TFA, TCA, TFA + DCM, TFA + CHCl₃ and TFA + DMF are in a good agreement with the theoretical prediction for entangled solutions in a good solvent [33].

It has been shown that there needs to be a minimum level of chain entanglements, therefore a minimum polymer concentration, for the formation of nanofibres in pressurised gyration [1]. A minimum polymer concentration known as the critical chain entanglement concentration (C_e) is thus a prerequisite to form the nanofibres. Below C_e only polymer beads or droplets were obtained. For PET in good solvents the C_e value was determined to be 20 wt%. Below this value only polymer beads were obtained. These are consistent with the previous results obtained in pressurised gyration experiments [1,4]; however, the minimum polymer concentration values needed to form nanofibres are different for various polymers. The degree of polymer chain entanglement for spinning the nanofibres differs with molecular weight and the solvent/solvent systems used for a polymer. The degree of swelling depends on the polymer–solvent interaction at a given temperature and the humidity for a polymer. Therefore, the chain geometry of the polymer varies and the critical chain entanglement concentration varies for different polymers [34].

3.4. Mathematical model for scaling of fibre diameter

An analytical model which allows the prediction of the generated fibre diameter based on various parameters involved in pressurised gyration was developed. This is the first time modelling of pressurised gyration for fibre production has been attempted. To make the derivation more practical and effective it was divided into a rotational frame and blowing frame where the centrifugal force is a dominant factor in the former and the dynamic fluid flow in the latter. In the rotational frame, a section of a fibre that lies between the orifice and the collector of the vessel was considered. The equation of continuity along the direction x results in the equation:

$$Ur_1^2 = Vr_2^2 \tag{1}$$

where U is the initial velocity, r_1 initial jet radius, V is the final velocity and r_2 is the final jet radius.

Balancing the momentum in the x-direction in the steady state gives:

$$V^2 A = \frac{3\mu A}{\rho}\frac{dv}{dx} + \frac{\sigma\sqrt{A}}{\rho} - A\Omega^2 x \tag{2}$$

where μ is viscosity, ρ is density, σ is surface tension, A is jet cross-sectional area and Ω is angular velocity.

In the blowing frame a section of a fibre that lies between the orifice and the collector of the vessel was considered. The momentum balance along the direction x in the steady state gives:
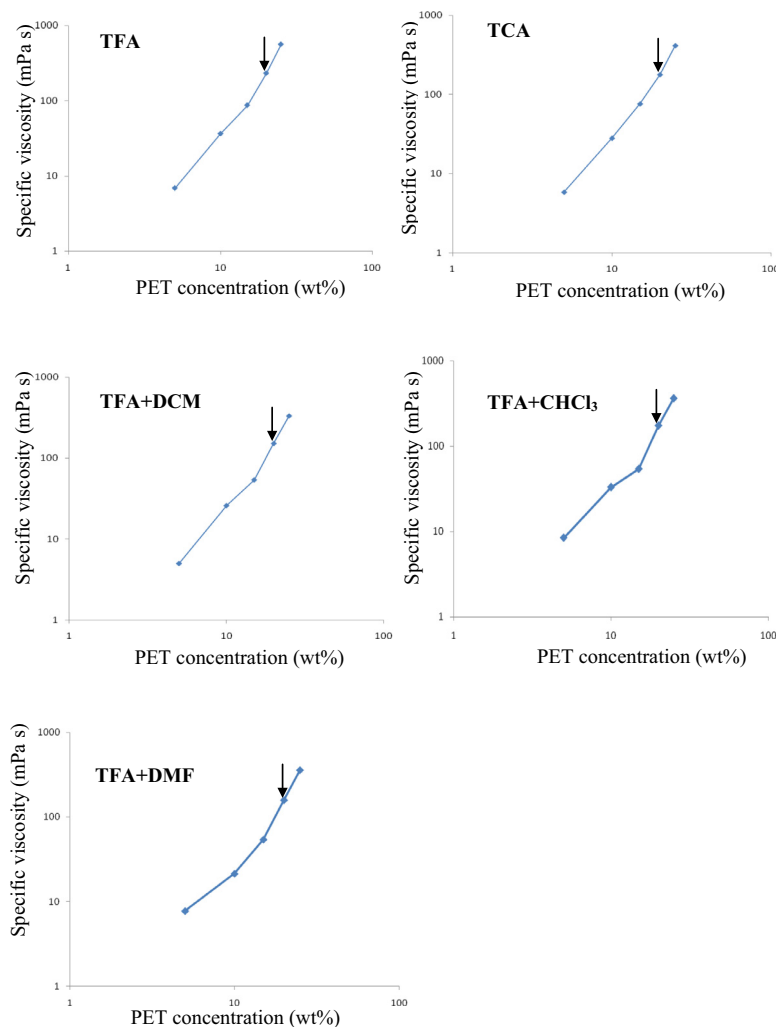
Fig. 4. Plots of specific viscosity and PET concentration in good solvents. Each arrow in the plots indicates the transition from semi-dilute unentangled to semi-dilute entangled.

Table 3
PET solubility, scaling relationships and fibre diameter and the morphology obtained by pressurised gyration at a rotating speed 36,000 rpm and working pressure 1×10^5 Pa, for various solvents used in this work.

Solvent	Solubility	Scaling relationships		Fibre diameter (nm)	Morphology
		Unentangled region	Entangled region		
TFA	Higher	$\sim C^{2.3}$	$\sim C^{3.9}$	290 ± 42	Continuous and smooth fibres without beads
TCA	Higher	$\sim C^{2.3}$	$\sim C^{3.7}$	310 ± 36	Continuous beaded fibres
TFA + DCM	Partial to higher	$\sim C^{2.1}$	$\sim C^{3.5}$	300 ± 35	Continuous beaded fibres
TFA + CHCl$_3$	Higher	$\sim C^{1.9}$	$\sim C^{3.7}$	714 ± 36	Networked and fused fibres
TFA + DMF	Higher	$\sim C^{1.7}$	$\sim C^{3.7}$	675 ± 35	Networked and fused fibres

$$V^2 A = \frac{3\mu A}{\rho}\frac{dV}{dx} + \pi r^2 \rho g - \pi \rho_a C_f r (V_a - V)^2 - Q\rho \frac{dV}{dx} \qquad (3)$$

where ρ_a is air density, C_f is air friction drawing coefficient, V_a is air velocity, Q is polymer mass flow rate and r is jet radius. g is acceleration due to gravity.

Combining Eqs. (2) and (3), and replacing the derivatives by ratios gives:

$$r_2 = \frac{r_1 U^{3/2} v^{1/2}}{R_c^{3/2} \Omega V_a} \qquad (4)$$

where $v = \frac{\mu}{\rho}$ is kinematic viscosity, R_c is radius of the collector.

This allows the scaling of fibre diameter as a function of fibre velocity, air velocity, kinematic viscosity, angular velocity of the vessel and the collector to vessel radius.

From the above equations it is seen that fibre radius is determined by competition between viscosity, surface tension, rotating speed and air velocity. From our previous work we have shown experimentally that key variables viscosity, rotating speed and working pressure influences the fibre radius [1]. Therefore, in this very first model for the pressurised gyration process only viscosity, rotating speed and air velocity were varied to determine the effect on fibre diameter. This strategy fitted well with the perturbation of the equations and gives the fibre radius value ~538 nm at the maximum values of the key variables which were taken to be 232 mPa s, 36,000 rpm and 30 m s^{-1}.
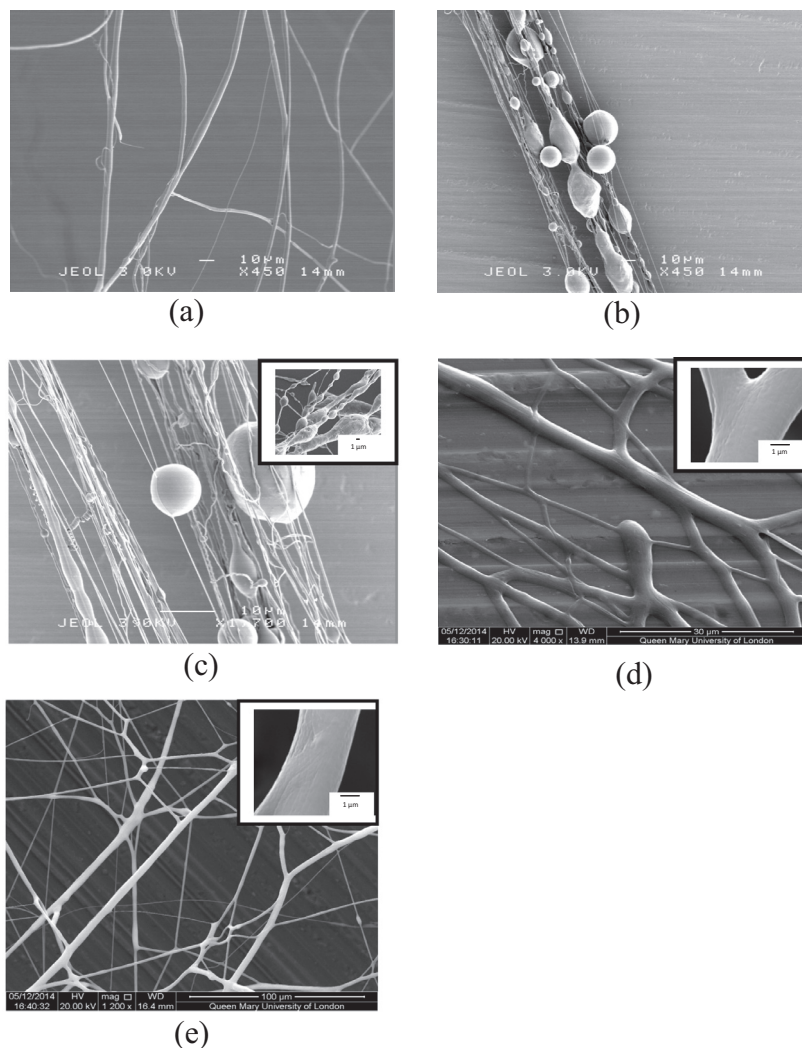
Fig. 5. Effect of solubility on nanofibre morphology. Scanning electron micrographs were taken from the nanofibres obtained using (a) TFA (b) TCA (c) TFA + DCM (d) TFA + CHCl₃ (e) TFA + DMF. Insets shows the high magnification scanning electron micrographs taken from nanofibres obtained using binary solvent systems.

3.5. Morphology of produced PET nanofibres

All the nanofibres were spun under identical conditions. The rotating speed was kept at 36,000 rpm and the working pressure was 0.1 MPa. Micrographs obtained for the 20 wt% polymer concentration for all solvents (Fig. 5) which demarcates a boundary between the semi-dilute unentangled and the semi-dilute entangled regime show that continuous bead-free nanofibres and the beaded nanofibres were obtained for single solvents TFA and TCA, respectively. The binary solvent system TFA + DCM gave beaded morphology, whereas TFA + CHCl₃ and TFA + DMF showed bead-free fibres (Fig. 5). In these cases nanofibres appeared smooth and uniform. The interconnection of nanofibres led to formation of a network-like structure. This may be due to a "fingering instability" at the orifice of the gyration vessel that may not have sufficient shear force to break-off as individual nanofibres. The fusion of polymer nanofibres at junctions may be due to solvent evaporation and the variation in solvent evaporation rate in the binary solvent system. The lower boiling solvent has little time to evaporate and solidifies quickly during the spinning process resulting in fusion of fibres at the junction. The mean fibre diameters were measured to be 290 ± 42, 310 ± 36, 300 ± 35, 714 ± 36, 675 ± 35 nm for TFA, TCA,
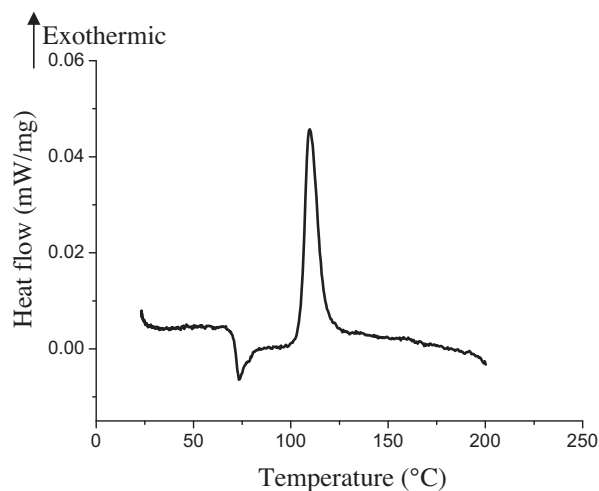

Fig. 6. DSC trace obtained from the PET nanofibres produced by pressurised gyration, the TGA of the same temperature span did not reveal any appreciable weight loss. Conditions: 20 w% PET in TFA spun at 36,000 rpm and 0.1 MPa working pressure.

TFA + DCM, TFA + CHCl₃ and TFA + DMF solvents, respectively (Table 3).

The actual/predicted fibre diameters are in the range 0.54–1.26. It is therefore clear that the present model only allows scaling the nanofibre diameter and also does not take into account the different morphological features such as porosity and, in particular, surface roughness. Attempts to refine the present model so that it can be applied more specifically to different polymer–solvent systems requires the incorporation of system dependent specific properties such as adsorption force, surface rheology and roughness, pore size and volume.

Pressurised gyration of nanofibres is influenced by the rotating speed of the vessel, working pressure and polymer concentration. Generally, increasing the rotating speed and the working pressure reduce the fibre diameter [1,2,4]. The fibre diameter distribution is also affected by those parameters giving more homogeneous fibres. A higher polymer concentration increases the chance of formation of nanofibres. However, that is not always the case, unless the polymer solutions have a sufficient amount of chain entanglements [4]. It has been shown that below a certain value of polymer concentration only beaded structures were obtained [1]. The bead-on-string and continuous fibre morphology were obtained when increasing the polymer concentration above a certain value. It is interesting to see that TFA gives bead free continuous fibres whereas TCA and TFA + DCM give continuous beaded fibre morphology. Fibre fusion and a network structure have been obtained for TFA + DMF and TFA + CHCl₃. It has been reported that solvent properties such as boiling point, density, surface tension and viscosity influence nanofibre morphology [35]. Comparatively, TFA has a moderate boiling point, TCA has a high boiling point and DCM has a low boiling point (Table 4). Generally, solvents with a high boiling point evaporate slowly and this causes stretching of the polymeric jet during pressurised gyration [36]. It is also noteworthy that defect-free nanofibre morphologies could be produced when the concentration is 2–2.5 times the C_e value [32]. Thus, the beaded nanofibres obtained for TCA and TFA + DCM solvents shows that the 20 wt% is in the transition regime for the entangled network but below the concentrated regime where a strong overlapping of polymer molecules occur to form bead-free nanofibres.

The insets in Fig. 5(c)–(e) show higher magnification images of the nanofibres formed in the binary solvent systems. Porous structures are visible at the surface of nanofibres obtained for the TFA + DCM solvent system (Fig. 5(c)). For TFA + CHCl₃ and TFA + DMF solvent systems the surface appears rougher and there are no apparent pores (Fig. 5(d) and (e)). Generally, phase separation in a binary solvent system results in pore formation in nanofibres [37]. Solvents with high volatility and vapour pressure cause phase separation and surface porosity in spun nanofibres. By decreasing solvent volatility, porosity and smoothness of the surface of the fibres could be controlled [37]. When two solvents have different boiling points the evaporation rates of the solvents vary during the stretching and cooling process in fibre formation. This leads to a solvent-rich phase and a solvent-poor phase giving rise to the porous structure. In addition, the mixing of polymer in a binary solvent system which consists of a good polymer solvent and a non-solvent can lead to a polymer-rich and a polymer-poor region causing phase separation to form porous structures [38]. It has been reported that the water vapour in the air could also lead to phase separation resulting in porosity in the bulk of the fibres [39]. At high humidity the water vapour which is a non-solvent to a polymer might diffuse and form liquid–liquid phase separation leading to porous structures. Moreover, the surface can develop porosity due to formation of breath figures [40]. Good miscibility of a polymer solvent and a non-solvent can facilitate precipitation during collection and solidification of nanofibres thus forming the porous structures. Blended polymeric structures have been shown

to be porous by selectively removing one component from the other without controlling the ambient conditions [41]. Also, it is known that nucleation and growth during phase separation results in pores on the fibre surface, while spinoidal decomposition can result in wrinkled fibre morphology [42]. But none of these case-specific reasons are thought to be the cause of the fibre morphologies observed in this work where a very different processing and forming route (pressurised gyration) was used.

It has been demonstrated recently that, solvent volatility has a significant influence on fibre morphology [43]. Based on the information from the Teas graph the solvent ratio can be calculated for the binary solvent system. Comparatively, the TFA + DCM has a 1:1 volume ratio and has moderate to low boiling points, thus it has a high volatility which may have formed the porous structures. On the other hand TFA + CHCl₃ and TFA + DMF has moderate to high boiling points and with a volume ratio of 4:1. It is unlikely that the solid porous structures obtained for this composition were caused by the low volatility of the solvents. Further experimental investigations and theoretical calculations on the temperature change, solvent evaporation rate and humidity which can determine the overall quality of the solvent as well as cooling and solidification processes need to be explored to be more conclusive about morphological change.

3.6. Fibre characteristics

Fig. 6 shows the heating scan of the as spun PET nanofibres obtained from pressurised gyration under optimised conditions. In general, the shape of the DSC trace contains the peaks of glass transition, crystallisation and melting of nanofibres. A glass transition of 73 °C and a cold crystallisation of 110 °C were obtained for the nanofibres. The glass transition temperature is slightly lower than the raw PET value reported (78 °C) and this is due to masking of endothermic relaxation in the spun PET nanofibres [10]. The cold crystallisation peak shows that the nanofibres contain a
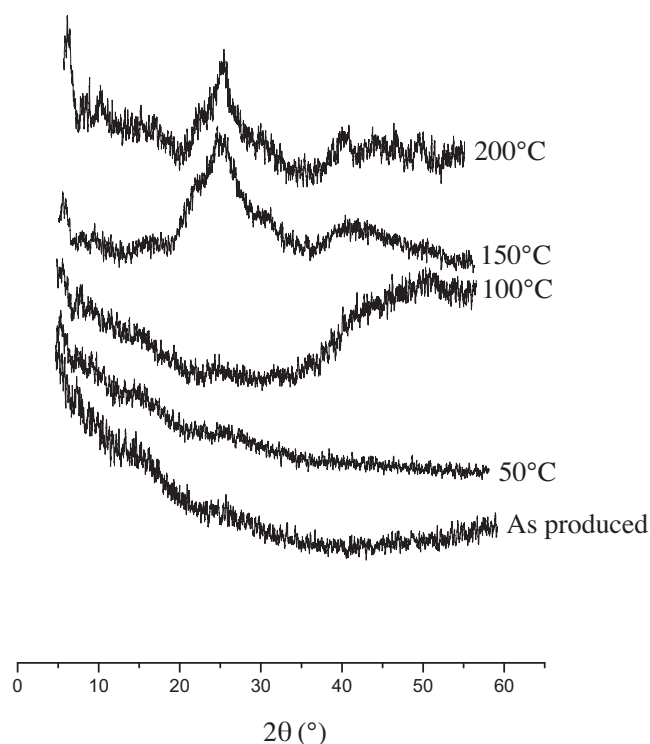

Fig. 7. XRD patterns of the PET nanofibres produced under conditions given in Fig. 6 and annealed at various temperatures (indicated).

Table 4
Boiling point and other physical properties of the solvents used to obtain PET nanofibres in pressurised gyration [45–47].

Solvent	Boiling point (°C)	Viscosity (mPa s)	Surface tension (mN/m)
TFA	72.3	0.93	16
TCA	196	0.88	14
DCM	39.6	0.44	28
DMF	153	0.82	35
CHCl$_3$	61	0.57	27

crystallisable free amorphous region. The enthalpy change associated with the crystallisation exotherm is ~10 J/g which is much lower than that of raw PET and indicates that the as-spun nanofibres already consists of a smaller amount of crystallisable free amorphous region. A careful examination of curve also reveals that there is an enthalpy recovery at 82 °C with an endothermic enthalpy of ~5 J/g. TGA experiments of these PET nanofibres showed that there is no weight loss observed for fibres over the temperature range of 200 °C. It indicates that nanofibres are highly hydrophobic and hence no moisture is present on the surface. It is also suggesting that the nanofibres are well dried when deposited on the collector. Thus, the solvent was completely removed during fibre solidification.

The XRD patterns of PET nanofibres annealed at various temperatures are shown in Fig. 7. The as-spun nanofibres do not show any detectable peaks. Upon annealing, no apparent variation in the XRD patterns is observed. Nanofibres annealed above 100 °C exhibits a crystalline X-ray pattern with well defined reflections. This is consistent with the above DSC trace obtained for PET nanofibres. The prominent peak at $2\theta \approx 26°$ is a characteristic peak of PET corresponding to the triclinic unit cell [21]. The sharpness of the peak increased with annealing temperature. The broadness of peak decreased with annealing temperature suggesting finer crystallites are formed. The control of crystal phases in PET nanofibres in this way can lead to applications such as those sought after in drug delivery [44].

4. Conclusions

The solubility–spinnability map for PET based on solubility parameters for various solvents was developed on a Teas graph and the successful spinnability region of nanofibres produced by pressurised gyration was identified. This region was used to develop a binary solvent system that would allow the formation of nanofibres in pressurised gyration. This new solubility–spinnability map simplified the solvent selection process by allowing mixed solvent systems to be developed. A high solubility of PET is required for the formation of nanofibres in pressurised gyration, otherwise polymer beads are obtained. Furthermore, a correlation between the rheological properties and the spinnability of the nanofibres in pressurised gyration based on critical minimum polymer concentration and chain entanglement was deduced. The specific viscosity of PET is proportional to ~C$^{3.9}$, C$^{3.7}$, C$^{3.5}$, C$^{3.7}$ and C$^{3.7}$ in the semidilute entangled regime for good solvents. A mathematical model consisting of rotational and blowing frames was developed to successfully scale the fibre diameter with the experimental parameters. The predicted fibre diameter is reasonably close to the values obtained in experiments. The nanofibre morphology showed a continuous defect free structure for TFA and a beaded nanofibre structure for TCA and the binary solvent system containing TFA + DCM. The high volatility and high vapour pressure induced surface porosity for fibres made with the binary solvent system TFA + DCM. The binary solvent systems TFA + CHCl$_3$ and TFA + DMF gave pore-free dense structures inhibiting phase separation. Thermal analysis showed a cold crystallisation

temperature of 110 °C for the spun nanofibres. There is no apparent weight loss observed for the prepared nanofibres and confirms that the nanofibres produced are solvent free. PET nanofibres were amorphous but crystallisation can be induced and controlled by annealing.

References

[1] S. Mahalingam, M. Edirisinghe, Forming of polymer nanofibres by a pressurised gyration process, Macromol. Rapid Commun. 34 (2013) 1134–1139.
[2] B.T. Raimi-Abraham, S. Mahalingam, M. Edirisinghe, D.Q.M. Craig, Generation of poly(N-vinylpyrrolidone) nanofibres using pressurised gyration, Mater. Sci. Eng., C 39 (2014) 168–176.
[3] S. Mahalingam, B.T. Raimi-Abraham, D.Q.M. Craig, M. Edirisinghe, Formation of protein and protein-gold nanoparticle stabilized microbubbles by pressurized gyration, Langmuir 31 (2015) 659–666.
[4] S. Mahalingam, G.G. Ren, M. Edirisinghe, Rheology and pressurised gyration of starch and starch-loaded polyethylene oxide, Carbohydr. Polym. 114 (2014) 279–287.
[5] S. Mahalingam, G. Pierin, P. Colombo, M. Edirisnghe, Facile one-pot formation of ceramics fibres from preceramic polymers by pressurised gyration, Ceram. Int. 41 (2015) 6067–6073.
[6] P.C. Hiemenz, Polymer Chemistry: The Basic Concepts, Marcel Dekker Inc., New York, 1984.
[7] H. Fong, I. Chun, D.H. Reneker, Beaded nanofibers formed during electrospinning, Polymer 40 (1999) 4585–4592.
[8] C.J. Luo, S.D. Stoyanov, E. Stride, E. Pelan, M. Edirisinghe, Electrospinning versus fibre production methods: from specifics to technological convergence, Chem. Soc. Rev. 41 (2002) 4708–4735.
[9] J.F. Zheng, A.H. He, J.X. Li, C.C. Han, Polymorphism control of poly(vinylidene fluoride) through electrospinning, Macromol. Rapid Commun. 28 (2007) 2159–2162.
[10] B. Veleirinho, M.F. Rei, J.A. Lopes-Da-Silva, Solvent and concentration effects on the properties of electrospun poly(ethylene terephthalate) nanofiber mats, J. Polym. Sci. Polym. Phys. 46 (2008) 460–471.
[11] C.J. Luo, M. Nangrego, M. Edirisinghe, A novel method of selecting solvents for polymer electrospinning, Polymer 51 (2010) 1654–1662.
[12] C.J. Luo, E. Stride, M. Edirisinghe, Mapping the influence of solubility and dielectric constant on electrospinning polycaprolactone solutions, Macromolecules 45 (2012) 4669–4680.
[13] I. Stanescu, L.E.K. Achenie, A theoretical study of solvent effects on Kolbe–Schmitt reaction kinetics, Chem. Eng. Sci. 61 (2006) 6199–6212.
[14] T. Hashimoto, M. Shibayama, H. Kawai, Ordered structure in block polymer-solutions. 4. Scaling rules on size of fluctuations with block polymer-weight, concentration, and temperature in segregation and homogenous regimes, Macromolecules 16 (1983) 1093–1101.
[15] T. Inoue, T. Soen, H. Kawai, M. Fukatsu, M. Kurata, Electron microscopic texture of A-B type block copolymers of isoprene with styrene, J. Polym. Sci. B 6 (1968) 75.
[16] C.M. Hansen, Hansen Solubility Parameters 'A user's Handbook', second ed., CRC Press Inc., Boca Raton, Florida, 2007.
[17] A.E. Ozcam, K.E. Roskov, R.J. Spontak, J. Genzer, Generation of functional PET microfibers through surface-initiated polymerization, J. Mater. Chem. 22 (2012) 5855–5864.
[18] A. Mahendrasingam, C. Martin, W. Fuller, D.J. Blundell, R.J. Oldman, D.H. MacKerron, J.L. Harvie, C. Riekel, Observation of a transient structure prior to strain-induced crystallization in poly(ethylene terephthalate), Polymer 41 (2000) 1217–1221.
[19] M. Monier, D.A. Abdel-Latif, Synthesis and characterization of ion-imprinted chelating fibers based on PET for selective removal of Hg^{2+}, Chem. Eng. J. 221 (2013) 452–460.
[20] Z. Ma, M. Kotaki, T. Yong, W. He, S. Ramakrishna, Surface engineering of electrospun polyethylene terephthalate (PET) nanofibers towards development of a new material for blood vessel engineering, Biomaterials 26 (2005) 2527–2536.
[21] K. Sreelatha, P. Predeep, Electrically conducting plastic films from polyethylene terephthalate for optoelectronic applications, Polym. Sci. A 8 (2013) 480–486.
[22] C. Chen, L. Wang, Y. Huang, Ultrafine electrospun fibers based on stearate/polyethylene terephthalate composite as form stable phase change materials, Chem. Eng. J. 150 (2009) 269–274.
[23] J. Wang, D. Langhe, M. Ponting, G.E. Wnek, L.T.J. Korley, E. Baer, Manufacturing of polymer continuous nanofibers using a novel co-extrusion and multiplication technique, Polymer 55 (2014) 673–685.

[24] C. Wang, M.-F. Lee, Y.-J. Wu, Solution-electrospun poly(ethylene terephthalate) fibers: processing and characterisation, Macromolecules 45 (2012) 7939–7947.

[25] A.F.M. Barton, Handbook of Solubility Parameters and Other Cohesion Parameters, CRC Press Inc., Boca Raton, Florida, 1983 (chapter 8).

[26] J. Burke, C. Jensen (Eds.), AIC Book and Paper Group Annual, vol. 3, 1984, pp. 13–58.

[27] S.L. Shenoy, W.D. Bates, H.L. Frisch, G.E. Wnek, Role of chain entanglements on fiber formation during electrospinning of polymer solutions: good solvent, non-specific polymer–polymer interaction limit, Polymer 46 (2005) 3372–3384.

[28] Y. Eom, B.C. Kim, Solubility parameter-based analysis of polyacrylonitrile solutions in N,N-dimethyl formamide and dimethyl sulfoxide, Polymer 55 (2014) 2570–2577.

[29] J. Liu, T. Liu, S. Kumar, Effect of solvent solubility parameter on SWNT dispersion in PMMA, Polymer 46 (2005) 3419–3424.

[30] R.H. Colby, L.J. Fetters, W.G. Funk, W.W. Graessley, Effects of concentration and thermodynamic interaction on the viscoelastic properties of polymer-solutions, Macromolecules 24 (1991) 3873–3882.

[31] S. Chisca, A.I. Barzic, I. Sava, N. Olaru, M. Burma, Morphological and rheological insights on polyimide chain entanglements for electrospinning produced fibers, J. Phys. Chem. B 116 (2012) 9082–9088.

[32] M.G. McKee, G.L. Wilkes, R.H. Colby, T.E. Long, Correlations of solution rheology with electrospun fiber formation of linear and branched polyesters, Macromolecules 37 (2004) 1760–1767.

[33] P.G. De Gennes, Scaling Concepts in Polymer Physics, Cornell University Press, Ithaca, NY, 1979 (part A, section III).

[34] E. Antoniou, P. Alexandridis, Polymer conformation in mixed aqueous–polar organic solvents, Eur. Polym. J. 46 (2010) 324–335.

[35] J.M. Deitzel, J.D. Kleinmeyer, D. Harris, N.C.M. Tan, The effect of processing variables on the morphology of electrospun nanofibers and textiles, Polymer 42 (2001) 261–272.

[36] C.L. Pai, M.C. Boyce, G.C. Rutledge, Morphology of porous and wrinkled fibers of polystyrene electrospun from dimethylformamide, Macromolecules 42 (2009) 2102–2114.

[37] S. Megelski, J.S. Stephens, D.B. Chase, J.F. Rabolt, Micro-nanostructured surface morphology on electrospun polymer fibres, Macromolecules 35 (2002) 8456–8466.

[38] P. van de Witte, P.J. Dijkstra, J.W.A. van den Berg, J. Feijen, Phase separation processes in polymer solutions in relation to membrane formation, J. Membr. Sci. 117 (1996) 1–31.

[39] P. Dayal, J. Liu, S. Kumar, T. Kyu, Experimental and theoretical investigations of porous structure formation in electrospun fibres, Macromolecules 40 (2007) 7689–7694.

[40] C.L. Casper, J.S. Stephens, N.G. Tassi, D.B. Chase, J.F. Rabolt, Macromolecules 37 (2004) 573–578.

[41] M. Bognitzki, T. Frese, M. Steinhart, A. Greiner, J.H. Wendorff, A. Schaper, Preparation of fibers with nanoscaled morphologies: electrospinning of polymer blends, Polym. Eng. Sci. 41 (2001) 982–991.

[42] H. Fashandi, M. Karimi, Pore formation in polystyrene fibre by superimposing temperature and relative humidity of electrospinning atmosphere, Polymer 53 (2012) 5832–5849.

[43] L. Li, Z. Jiang, M. Li, R. Li, T. Fang, Hierarchically structured PMMA fibres fabricated by electrospinning, RSC Adv. 4 (2014) 52973–52985.

[44] J.-C. Jeong, J. Lee, K. Cho, Effects of crystalline microstructure on drug release behaviour of poly(epsilon-caprolactone) microspheres, J. Control. Release 92 (2003) 249–258.

[45] Y. Marcus, The Properties of Solvents, John Wiley & Sons, Chichester, 1998 (chapter 3).

[46] M. Ash, I. Ash, The Index of Solvents, Gower Publishing, Hampshire, 1996. pp. 1–587.

[47] E.W. Flick, Industrial Solvent Handbook, William Andrew Publishing, New Jersey, 1998. pp. 1–937.